

# Application of Metal-Metalloid Oxide for Energy Production in Nano-Biofuel Cells: A First-Principles DFT Modeling

Fatemeh Mollaamin<sup>1,\*</sup> 

<sup>1</sup> Department of Biomedical Engineering, Faculty of Engineering and Architecture, Kastamonu University, Kastamonu, Turkey

\* Correspondence: [fmollaamin@kastamonu.edu.tr](mailto:fmollaamin@kastamonu.edu.tr);

Received: 2.01.2025; Accepted: 19.07.2025; Published: 30.09.2025

**Abstract:** With the pressure for renewable energy resources and the increasingly digitalized current lifestyle, the need for batteries will increase. Therefore, this article has evaluated promising alternative alkali metals for sodium-ion and potassium-ion batteries. A comprehensive investigation on hydrogen grabbing by  $\text{Li}_2[\text{SiO-SnO}]$ ,  $\text{Na}_2[\text{SiO-SnO}]$ , or  $\text{K}_2[\text{SiO-SnO}]$  was carried out using density functional theory (DFT). The values detect that with adding lithium, sodium and potassium, the negative atomic charge of oxygen atoms of O2, O3, O7–O12, O14, O15, O17, O18, O22–O27, O29, O30 in  $\text{Li}_2[\text{SiO-SnO}]-2\text{H}_2$ ,  $\text{Na}_2[\text{SiO-SnO}]-2\text{H}_2$  or  $\text{K}_2[\text{SiO-SnO}]-2\text{H}_2$  nanoclusters increases. The differences of charge density for these structures are measured as:  $\Delta Q_{\text{Li}_2[\text{SiO-SnO}]} = -0.002$ ,  $\Delta Q_{\text{Na}_2[\text{SiO-SnO}]} = -0.009$ , and  $\Delta Q_{\text{K}_2[\text{SiO-SnO}]} = -0.00$ . Therefore, the results have shown that the cluster of  $\text{Na}_2[\text{SiO-SnO}]$  and  $\text{Li}_2[\text{SiO-SnO}]$  may have the highest electron-accepting ability owing to hydrogen grabbing. The hypothesis of the hydrogen adsorption phenomenon was confirmed by density distributions of CDD, TDOS, and ELF for nanoclusters of  $\text{Li}_2[\text{SiO-SnO}]-2\text{H}_2$ ,  $\text{Na}_2[\text{SiO-SnO}]-2\text{H}_2$ , or  $\text{K}_2[\text{SiO-SnO}]-2\text{H}_2$ . The fluctuation in charge density values demonstrates that the electronic densities were mainly located in the boundary of adsorbate/adsorbent atoms during the adsorption status. The advantages of lithium, sodium, or potassium over Si/ Sn are that they possess higher electron and hole mobility, allowing lithium, sodium, or potassium instruments to operate at higher frequencies than Si/ Sn instruments.

**Keywords:** semiconductor alloys; surface science; density of states; charge distribution; adsorption model; energy-saving.

© 2025 by the authors. This article is an open-access article distributed under the terms and conditions of the Creative Commons Attribution (CC BY) license (<https://creativecommons.org/licenses/by/4.0/>), which permits unrestricted use, distribution, and reproduction in any medium, provided the original work is properly cited. The authors retain copyright of their work, and no permission is required from the authors or the publisher to reuse or distribute this article, as long as proper attribution is given to the original source.

## 1. Introduction

With the increasing global demand for energy, there is an essential need for alternative, efficient energy storage systems. This is driving research into non-lithium battery systems. This paper presents comprehensive research on non-lithium battery technologies, specifically sodium-ion and potassium-ion batteries [1–10]. Along with sodium ion, potassium ion is the prime chemistry replacement candidate for lithium-ion batteries. Potassium-ion has certain advantages over similar lithium-ion, such as the cell design being simple and both the material and the fabrication procedures being cheaper. The key advantage is the abundance and low cost of potassium in comparison with lithium, which makes potassium batteries a promising candidate for large-scale batteries such as household energy storage and electric vehicles.

Another advantage of a potassium-ion battery over a lithium-ion battery is potentially faster charging [11–20].

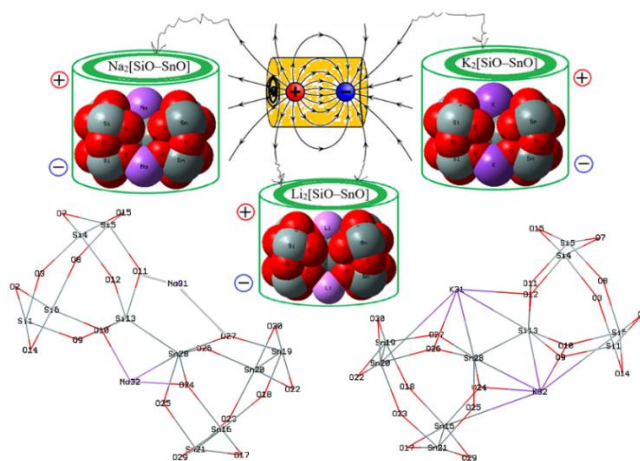
Recently, Si-, Ge-, or Sn-carbide nanostructures have been suggested as engaged H-grabbing compounds [21–32]. Since the polarizability of silicon is more than that of carbon, it is supposed that Si–C/Si nanosheet might attach to compositions more strongly in comparison to the net carbon nano-surfaces [33–41].

In our previous works, the investigation of energy storage in fuel cells through hydrogen adsorption has been accomplished using DFT calculations through different nanomaterials consisting of silicon/germanium/tin/lead nano-carbides, magnesium-aluminum alloy, and aluminum/carbon/ silicon doping boron nitride nanocage [42–44].

Nanomaterials with remarkable specific structures indicate promising applications in the field of energy storage, electrocatalysis, and fuel cells. Currently, the present research aims to explore the possibility of using  $\text{Li}_2[\text{SiO-SnO}]$ ,  $\text{Na}_2[\text{SiO-SnO}]$ , or  $\text{K}_2[\text{SiO-SnO}]$  nanocluster for hydrogen storage by employing first-principles calculations. We have analyzed the structural and electronic properties of  $\text{Li}_2[\text{SiO-SnO}]$ ,  $\text{Na}_2[\text{SiO-SnO}]$  or  $\text{K}_2[\text{SiO-SnO}]$  nanocluster and hydrogen-adsorbed nanoclusters of  $\text{Li}_2[\text{SiO-SnO}]-2\text{H}_2$ ,  $\text{Na}_2[\text{SiO-SnO}]-2\text{H}_2$  or  $\text{K}_2[\text{SiO-SnO}]-2\text{H}_2$ . using state-of-the-art computational techniques. The current manuscript provides focused research on these Li/Na/K incorporated cathode materials for Na/K/Li-ion batteries.

## 2. Materials and Methods

The idea of lithium/sodium/potassium incorporated cathodes for both Li/Na/K-ion batteries has gained significant consideration throughout the past decade. The encouraging performance of various reported Li/Na/K incorporated cathode systems has the potential to review the exciting developments made so far to clearly understand the effect of numerous variables in improving electrochemical performance. The goal of this study is to hydrogen adsorption by using alkali metals-based nanoclusters of  $\text{Li}_2[\text{SiO-SnO}]$ ,  $\text{Na}_2[\text{SiO-SnO}]$ , or  $\text{K}_2[\text{SiO-SnO}]$  (Figure 1), which can increase the hydrogen storage in cell batteries, transistors or other semiconductors. In our research, the calculations have been done by density functional theory (DFT) computations at the Coulomb-attenuating method–Becke, 3-parameter, Lee–Yang–Parr with Dispersion–corrected (CAM–B3LYP–D3/6–311+G (d,p)) level of theory [45].



CAM-B3LYP yields atomization energies of similar quality to those from B3LYP while also performing well for charge transfer excitations, which B3LYP underestimates enormously. Fig.1 shows the process of hydrogen adsorption by  $\text{Li}_2[\text{SiO-SnO}]$ ,  $\text{Na}_2[\text{SiO-SnO}]$  or  $\text{K}_2[\text{SiO-SnO}]$  nanocluster and hydrogen-adsorbed nanoclusters of  $\text{Li}_2[\text{SiO-SnO}]-2\text{H}_2$ ,  $\text{Na}_2[\text{SiO-SnO}]-2\text{H}_2$  or  $\text{K}_2[\text{SiO-SnO}]-2\text{H}_2$ . The Bader charge analysis [46,47] was discussed during the trapping of hydrogen atoms by  $\text{Li}_2[\text{SiO-SnO}]$ ,  $\text{Na}_2[\text{SiO-SnO}]$ , or  $\text{K}_2[\text{SiO-SnO}]$  nanoclusters (Figure 1). Bader charge analysis is a code for the analysis of charge density with an intuitive way of dividing molecules into atoms. Bader uses what are called zero flux surfaces to divide atoms [46,47]. The rigid potential energy surface using density functional theory [48–61] was performed due to the Gaussian 16 revision C.01 program package [62] and GaussView 6.1 [63]. The coordination input for hydrogen grabbing by  $\text{Li}_2[\text{SiO-SnO}]$ ,  $\text{Na}_2[\text{SiO-SnO}]$ , and  $\text{K}_2[\text{SiO-SnO}]$  has lanl2dz and applied 6-311+G (d,p) basis sets.

### 3. Results and Discussion

#### 3.1. Charge density differences analysis.

The amounts of charge density differences (CDD) [64] are measured by considering isolated atoms or noninteracting ones. The mentioned approximation can be the lightest to use because the superposition value may be received from the primary status of the self-consistency cycle in the code that carries out the density functional theory (Figure 2a, a', b, b', c, c').

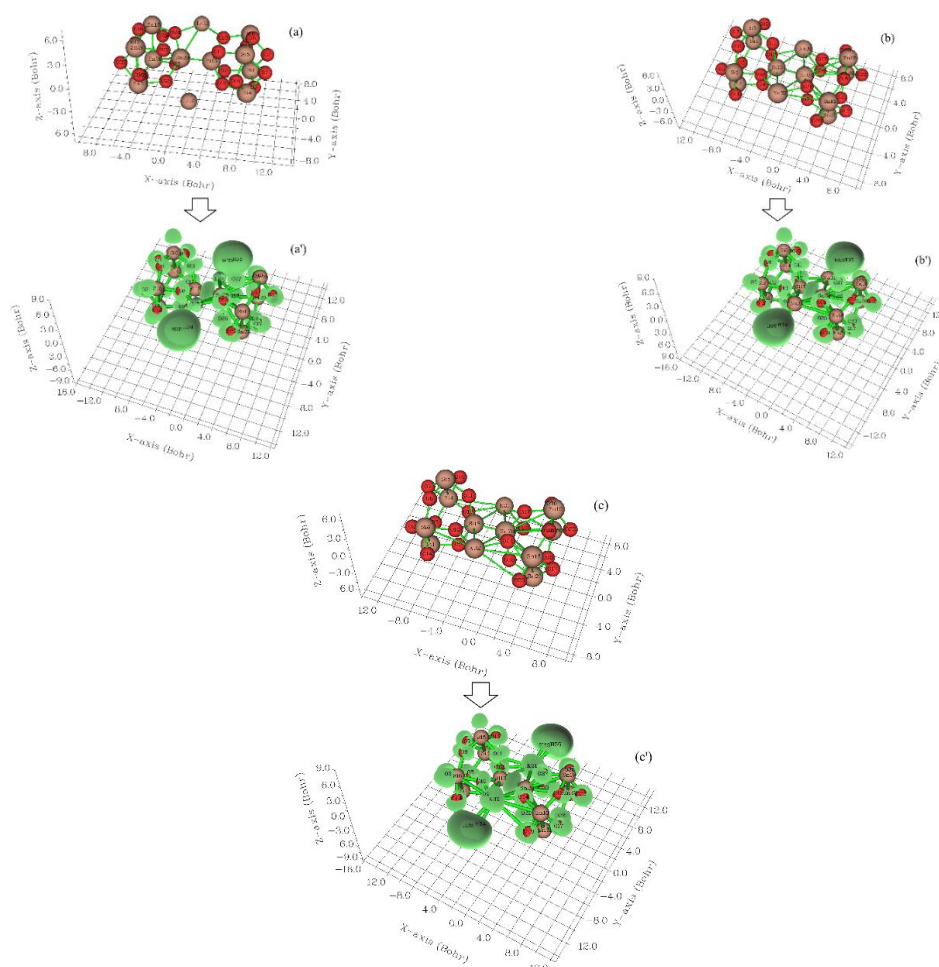


**Figure 2.** CDD graphs for (a)  $\text{Li}_2[\text{SiO-SnO}]$ ; (a')  $\text{Li}_2[\text{SiO-SnO}]-2\text{H}_2$ ; (b)  $\text{Na}_2[\text{SiO-SnO}]$ ; (b')  $\text{Na}_2[\text{SiO-SnO}]-2\text{H}_2$ ; (c)  $\text{K}_2[\text{SiO-SnO}]$ ; (c')  $\text{K}_2[\text{SiO-SnO}]-2\text{H}_2$  nanoclusters.

In Figure 2a,  $\text{Li}_2$  [SiO–SnO] cluster with the fluctuation in the region around  $-12$  to  $+6$  Bohr forms the nanocluster of  $\text{Li}_2[\text{SiO–SnO}]-2\text{H}_2$  (Fig. 2a') in the area around  $-12$  to  $+3$  Bohr. Furthermore, the atoms of O2, O3, O7–O12, O14, O15, O17, O18, O22–O27, O29, and O30 from  $\text{Na}_2$  [SiO–SnO] (Figure 2b) have shown the fluctuation around  $-12$  to  $+4$  Bohr towards formation of  $\text{Na}_2[\text{SiO–SnO}]-2\text{H}_2$  through hydrogen adsorption (Figure 2b'). In addition, the  $\text{K}_2$ [SiO–SnO] cluster with the fluctuation in the region around  $-12$  to  $+4$  Bohr (Figure 2c) forms the nanocluster of  $\text{K}_2[\text{SiO–SnO}]-2\text{H}_2$  during hydrogen grabbing (Figure 2c') in the same range of area around  $-12$  to  $+4$  Bohr. Atomic charge was discussed during trapping of hydrogens by  $\text{Li}_2$ [SiO–SnO],  $\text{Na}_2$ [SiO–SnO] or  $\text{K}_2$ [SiO–SnO] nanoclusters towards formation of  $\text{Li}_2$ [SiO–SnO]– $2\text{H}_2$ ,  $\text{Na}_2$ [SiO–SnO]– $2\text{H}_2$  or  $\text{K}_2$ [SiO–SnO]– $2\text{H}_2$ , respectively (Tables 1,2,3).

**Table 1.** The atomic charge (Q/coulomb) for the atomic charge (Q/coulomb) for  $\text{Li}_2$  [SiO–SnO] and  $\text{Li}_2$  [SiO–SnO]– $2\text{H}_2$  nanoclusters.

$\text{Li}_2[\text{SiO–SnO}]$		$\text{Li}_2[\text{SiO–SnO}]-2\text{H}_2$	
Atom	Charge	Atom	Charge
Si1	1.4573	Si1	1.4553
O2	-0.6344	O2	-0.6351
O3	-0.8302	O3	-0.8307
Si4	1.4127	Si4	1.4141
Si5	1.4358	Si5	1.4341
Si6	1.4682	Si6	1.4675
O7	-0.7257	O7	-0.7262
O8	-0.8375	O8	-0.8376
O9	-0.7850	O9	-0.7852
O10	-1.0023	O10	-0.9966
O11	-0.8108	O11	-0.8106
O12	-0.9495	O12	-0.9484
Si13	1.4092	Si13	1.4139
O14	-0.7621	O14	-0.7657
O15	-0.6962	O15	-0.6961
Sn16	1.6967	Sn16	1.6983
O17	-0.8091	O17	-0.8088
O18	-0.8840	O18	-0.8840
Sn19	1.6929	Sn19	1.6891
Sn20	1.6650	Sn20	1.6644
Sn21	1.6925	Sn21	1.6902
O22	-0.8436	O22	-0.8442
O23	-0.8919	O23	-0.8916
O24	-1.0461	O24	-1.0419
O25	-0.9047	O25	-0.9049
O26	-1.0012	O26	-0.9981
O27	-0.9401	O27	-0.9404
Sn28	1.7846	Sn28	1.7871
O29	-0.8839	O29	-0.8850
O30	-0.8610	O30	-0.8623
Li31	0.7057	Li31	0.6002
Li32	0.6790	Li32	0.5841
		H33	-0.0216
		H34	-0.0070
		H35	0.1229
		H36	0.1010

**Table 2.** The atomic charge (Q/coulomb) for the atomic charge (Q/coulomb) for Na<sub>2</sub>[SiO–SnO] and Na<sub>2</sub> [SiO–SnO]–2H<sub>2</sub> nanoclusters.

Na <sub>2</sub> [SiO–SnO]		Na <sub>2</sub> [SiO–SnO]–2H <sub>2</sub>	
Atom	Charge	Atom	Charge
Si1	1.4607	Si1	1.4593
O2	-0.6355	O2	-0.6360
O3	-0.8304	O3	-0.8308
Si4	1.4046	Si4	1.4067
Si5	1.4414	Si5	1.4399
Si6	1.4617	Si6	1.4642
O7	-0.7259	O7	-0.7262
O8	-0.8374	O8	-0.8375
O9	-0.7871	O9	-0.7873
O10	-0.9997	O10	-0.9963
O11	-0.8130	O11	-0.8125
O12	-0.9665	O12	-0.9657
Si13	1.3821	Si13	1.3886
O14	-0.7677	O14	-0.7704
O15	-0.7022	O15	-0.7025
Sn16	1.7081	Sn16	1.7104
O17	-0.8097	O17	-0.8091
O18	-0.8850	O18	-0.8848
Sn19	1.6980	Sn19	1.6954
Sn20	1.6640	Sn20	1.6662
Sn21	1.6977	Sn21	1.6949
O22	-0.8451	O22	-0.8453
O23	-0.8917	O23	-0.8912
O24	-1.0612	O24	-1.0584
O25	-0.9072	O25	-0.9070
O26	-1.0300	O26	-1.0277
O27	-0.9335	O27	-0.9337
Sn28	1.8213	Sn28	1.8369
O29	-0.9000	O29	-0.8913
O30	-0.8629	O30	-0.8636
Na31	0.7785	Na31	0.6955
Na32	0.6636	Na32	0.5764
		H33	-0.0261
		H34	-0.0092
		H35	0.0976
		H36	0.0802

**Table 3.** The atomic charge (Q/coulomb) for the atomic charge (Q/coulomb) for K<sub>2</sub>[SiO–SnO] and K<sub>2</sub> [SiO–SnO]–2H<sub>2</sub> nanoclusters.

K <sub>2</sub> [SiO–SnO]		K <sub>2</sub> [SiO–SnO]–2H <sub>2</sub>	
Atom	Charge	Atom	Charge
Si1	1.4624	Si1	1.4570
O2	-0.6361	O2	-0.7018
O3	-0.8295	O3	-0.8283
Si4	1.4046	Si4	1.4138
Si5	1.4401	Si5	1.4582
Si6	1.4615	Si6	1.4460
O7	-0.7257	O7	-0.6628
O8	-0.8319	O8	-0.8282
O9	-0.7862	O9	-0.7873
O10	-1.0556	O10	-1.0637
O11	-0.8084	O11	-0.8043
O12	-0.9863	O12	-0.9631
Si13	1.3583	Si13	1.3548
O14	-0.7718	O14	-0.7182

K <sub>2</sub> [SiO–SnO]		K <sub>2</sub> [SiO–SnO]–2H <sub>2</sub>	
Atom	Charge	Atom	Charge
O15	–0.7076	O15	–0.7797
Sn16	1.6953	Sn16	1.6941
O17	–0.8053	O17	–0.8042
O18	–0.8792	O18	–0.8785
Sn19	1.6956	Sn19	1.6945
Sn20	1.6553	Sn20	1.6574
Sn21	1.6987	Sn21	1.6947
O22	–0.8455	O22	–0.8460
O23	–0.8881	O23	–0.8874
O24	–1.1110	O24	–1.1122
O25	–0.9047	O25	–0.9056
O26	–1.0603	O26	–1.0608
O27	–0.9230	O27	–0.9247
Sn28	1.6830	Sn28	1.6925
O29	–0.8952	O29	–0.8976
O30	–0.8646	O30	–0.8653
K31	0.8884	K31	0.8432
K32	0.8731	K32	0.8584
		H33	–0.0564
		H34	–0.0387
		H35	0.0858
		H36	0.0647

The atomic charge of Si, Sn, O, and alkali metals of Li, Na, K, and hydrogen atoms absorbed on Li<sub>2</sub>[SiO–SnO], Na<sub>2</sub>[SiO–SnO], or K<sub>2</sub>[SiO–SnO] nanoclusters have been measured. The values detect that by adding lithium, sodium and potassium, the negative atomic charge of oxygen atoms of O2, O3, O7–O12, O14, O15, O17, O18, O22–O27, O29, O30 in Li<sub>2</sub>[SiO–SnO]–2H<sub>2</sub>, Na<sub>2</sub>[SiO–SnO]–2H<sub>2</sub> or K<sub>2</sub>[SiO–SnO]–2H<sub>2</sub> nanoclusters augments. In fact, Li<sub>2</sub>[SiO–SnO], Na<sub>2</sub>[SiO–SnO], or K<sub>2</sub>[SiO–SnO] nanoclusters have shown more efficiency than SiO–SnO cluster [30] for admitting the electron from electron donor of H33, H34, H35, and H36 (Tables 1,2,3).

The changes of charge density analysis in the adsorption process have illustrated that Li<sub>2</sub> [SiO–SnO] has shown the "Bader charge" of –1.631 coulomb before hydrogen adsorption and –1.633 coulomb after hydrogen adsorption. Moreover, the changes of charge density analysis for Na<sub>2</sub>[SiO–SnO] have shown the "Bader charge" of –1.626 coulomb before hydrogen adsorption and –1.635 coulomb after hydrogen adsorption. However, K<sub>2</sub>[SiO–SnO] has shown the "Bader charge" of –1.574 coulomb before hydrogen adsorption and after hydrogen adsorption. The differences of charge density for these structures are measured as:  $\Delta Q_{Li_2[SiO-SnO]} = -0.002$ ,  $\Delta Q_{Na_2[SiO-SnO]} = -0.009$  and  $\Delta Q_{K_2[SiO-SnO]} = -0.00$ . Therefore, the results have shown that the cluster of Na<sub>2</sub> [SiO–SnO] and Li<sub>2</sub> [SiO–SnO] may have the most tendency for electron accepting owing to hydrogen grabbing.

### 3.2. DOS/TDOS analysis.

Squirming the molecular orbital data owing to Gaussian graphs of unit altitude and entire width at "half maximum (FWHM)" of 0.3 eV by "GaussSum 3.0.2" have computed total density of states (TDOS) diagrams [65]. Regarding the adsorption behavior of hydrogen by Li<sub>2</sub>[SiO–SnO], Na<sub>2</sub>[SiO–SnO], or K<sub>2</sub>[SiO–SnO] nanoclusters, TDOS has been measured. This parameter can indicate the existence of important chemical interactions often on the convex side (Figure 3a,a',b,b',c,c').

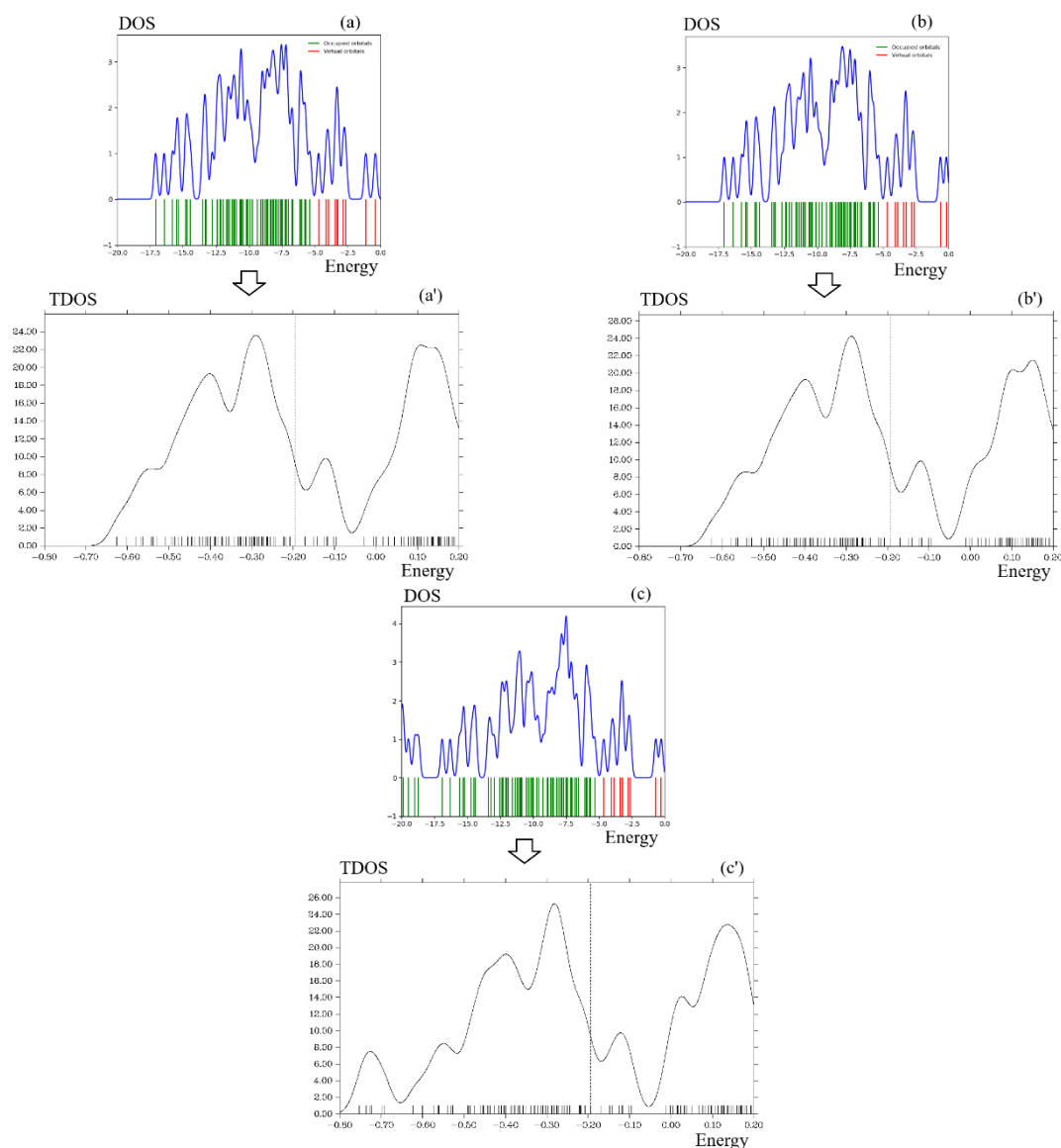


**Figure 3.** TDOS graphs of (a)  $\text{Li}_2[\text{SiO-SnO}]$ ; (a')  $\text{Li}_2[\text{SiO-SnO}]-2\text{H}_2$ ; (b)  $\text{Na}_2[\text{SiO-SnO}]$ ; (b')  $\text{Na}_2[\text{SiO-SnO}]-2\text{H}_2$ ; (c)  $\text{K}_2[\text{SiO-SnO}]$ ; (c')  $\text{K}_2[\text{SiO-SnO}]-2\text{H}_2$  nanoclusters.

During the formation of the  $\text{Li}_2[\text{SiO-SnO}]$  cluster, Figure 3a showed sharp and sophisticated peaks of around  $-0.3$ ,  $-0.45$ , and  $-0.60$  a.u. due to the covalent bond between two atoms of  $\text{Li}_2$  with  $\text{SiO-SnO}$  cluster. Moreover,  $\text{Li}_2[\text{SiO-SnO}]-2\text{H}_2$  has indicated a duplicate peak around  $-0.45$  to  $-0.5$  a.u. During hydrogen adsorption (Figure 3a'). After H-grabbing by  $\text{Na}_2[\text{SiO-SnO}]$  cluster, pointed peaks around  $-0.3$ ,  $-0.45$ , and  $-0.60$  a.u. due to a covalent bond between two atoms of Na with a  $\text{SiO-SnO}$  cluster (Figure 3b). Furthermore,  $\text{Na}_2[\text{SiO-SnO}]-2\text{H}_2$  has indicated a duplicate peak around  $-0.45$  to  $-0.5$  a.u. During hydrogen adsorption (Figure 3b'). However, the maximum energy of TDOS for  $\text{K}_2[\text{SiO-SnO}]$  (Figure 3c) with several peaks around  $-0.35$ ,  $-0.45$ ,  $-0.6$ , and  $-0.75$  a.u. with the maximum density of state of  $\approx 23$  around  $-0.35$  a.u. has been shown. Moreover, similar amounts of TDOS for  $\text{K}_2[\text{SiO-SnO}]-2\text{H}_2$  (Figure 3c') through some fluctuations in the behavior of the graphs have been observed.

### 3.3. Analysis of ELF.

A type of scalar field called electron localization function (ELF) may demonstrate a broad span of bonding samples. Nevertheless, the distinction between deduced/raised electron

delocalization/localization into cyclic  $\pi$ -conjugated sets stays encouraging for ELF [66]. The grosser the electron localization is in an area, the more likely the electron movement is restricted within it. Therefore, they might be discerned from the ones away if electrons are totally centralized. As Bader investigated, the zones with large electron localization possess extensive magnitudes of Fermi hole integration [67]. However, with a six-dimensional function for the Fermi hole, it seems hard to study directly. Then, Becke and Edgecombe remarked that spherically averaged spin conditional pair probability possesses a direct correlation with the Fermi hole and proposed the parameter of ELF in the Multiwfn program [68,69] and popularized for the spin-polarized procedure [70].

Regarding kinetic energy, ELF was rechecked to be more punctual for both Kohn-Sham DFT and post-HF wavefunctions [71]. In fact, the excess kinetic energy density caused by Pauli repulsion was unfolded by  $D(r)$ , and  $D_0(r)$  may be inspected as Thomas-Fermi kinetic energy density. Because  $D_0(r)$  brings forward the ELF as the origin, the ELF shows an affiliate localization. Trapping of hydrogens by  $\text{Li}_2[\text{SiO-SnO}]$ ,  $\text{Na}_2[\text{SiO-SnO}]$  or  $\text{K}_2[\text{SiO-SnO}]$  nanoclusters towards the formation of  $\text{Li}_2[\text{SiO-SnO}]-2\text{H}_2$ ,  $\text{Na}_2[\text{SiO-SnO}]-2\text{H}_2$  or  $\text{K}_2[\text{SiO-SnO}]-2\text{H}_2$  can be defined by ELF graphs owing to exploring their delocalization/localization characterizations of electrons and chemical bonds (Figure 4a,a',b,b',c,c').

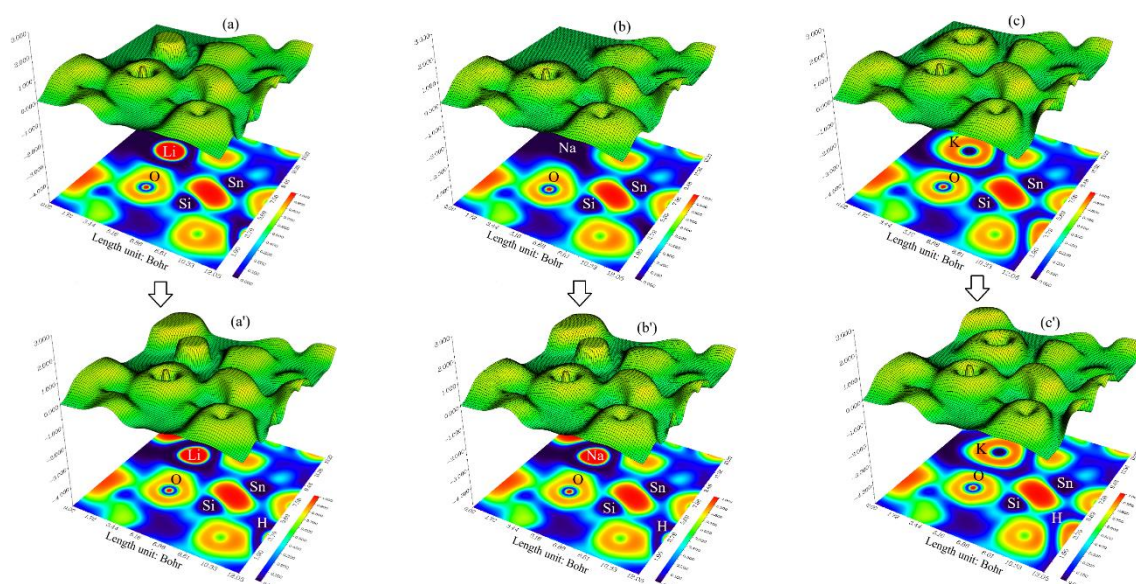


**Figure 4.** The counter map of ELF graphs for (a)  $\text{Li}_2[\text{SiO-SnO}]$ ; (a')  $\text{Li}_2[\text{SiO-SnO}]-2\text{H}_2$ ; (b)  $\text{Na}_2[\text{SiO-SnO}]$ ; (b')  $\text{Na}_2[\text{SiO-SnO}]-2\text{H}_2$ ; (c)  $\text{K}_2[\text{SiO-SnO}]$ ; (c')  $\text{K}_2[\text{SiO-SnO}]-2\text{H}_2$  nanoclusters.

A vaster jointed area engaged by an isosurface map has shown the electron delocalization in  $\text{Li}_2[\text{SiO-SnO}]$  (Figure 4a),  $\text{Li}_2[\text{SiO-SnO}]-2\text{H}_2$  (Figure 4a'),  $\text{Na}_2[\text{SiO-SnO}]$  (Figure 4b),  $\text{Na}_2[\text{SiO-SnO}]-2\text{H}_2$  (Figure 4b'),  $\text{K}_2[\text{SiO-SnO}]$  (Figure 4c), and  $\text{K}_2[\text{SiO-SnO}]-2\text{H}_2$  (Figure 4c') through labeling atoms of O12, Si13, O26, Ge28, X31(X=Li, Na or K) and H35. In fact, the counter map of ELF can confirm that  $\text{Li}_2[\text{SiO-SnO}]$ ,  $\text{Na}_2[\text{SiO-SnO}]$ , or  $\text{K}_2[\text{SiO-SnO}]$  nanocluster may increase the efficiency during hydrogen adsorption towards formation of  $\text{Li}_2[\text{SiO-SnO}]-2\text{H}_2$ ,  $\text{Na}_2[\text{SiO-SnO}]-2\text{H}_2$ , or  $\text{K}_2[\text{SiO-SnO}]-2\text{H}_2$  nanocluster.

Moreover, intermolecular orbital overlap integral is important in discussions of intermolecular charge transfer, which can calculate HOMO-HOMO and LUMO-LUMO overlap integrals between the  $\text{H}_2$  molecules and heteroclusters of  $\text{Li}_2[\text{SiO-SnO}]$ ,  $\text{Na}_2[\text{SiO-SnO}]$  or  $\text{K}_2[\text{SiO-SnO}]$ . The applied wavefunction level is CAM-B3LYP-D3/6-311+G (d, p), which corresponds to HOMO and LUMO, respectively (Table 4).

**Table 4.** LUMO, HOMO, energy gap ( $\Delta E$ ), Ring perimeter ( $\text{\AA}$ ), Total ring area ( $\text{\AA}^2$ ) for  $\text{Li}_2[\text{SiO-SnO}]$ ,  $\text{Na}_2[\text{SiO-SnO}]$ ,  $\text{K}_2[\text{SiO-SnO}]$  through hydrogen grabbing and formation of  $\text{Li}_2[\text{SiO-SnO}]-2\text{H}_2$ ,  $\text{Na}_2[\text{SiO-SnO}]-2\text{H}_2$ ,  $\text{K}_2[\text{SiO-SnO}]-2\text{H}_2$  heteroclusters.

Heteroclusters	Ring perimeter ( $\text{\AA}$ )	Total ring area ( $\text{\AA}^2$ )	Dipole moment (debye)	$E_{\text{HOMO}}$ (eV)	$E_{\text{LUMO}}$ (eV)	$\Delta E = E_{\text{LUMO}} - E_{\text{HOMO}}$ (eV)
$\text{Li}_2[\text{SiO-SnO}]$	9.3332	5.1566	5.1802	-5.3586	-4.7074	0.6512
$\text{Li}_2[\text{SiO-SnO}]-2\text{H}_2$	9.9121	6.6752	5.2403	-5.3156	-4.6649	0.6507
$\text{Na}_2[\text{SiO-SnO}]$	9.9122	6.6754	5.1335	-5.3163	-4.6563	0.6600
$\text{Na}_2[\text{SiO-SnO}]-2\text{H}_2$	9.9121	6.6752	5.1709	-5.2916	-4.6320	0.6596
$\text{K}_2[\text{SiO-SnO}]$	9.9122	6.6754	5.1012	-5.3109	-4.6247	0.6862
$\text{K}_2[\text{SiO-SnO}]-2\text{H}_2$	9.9121	6.6752	4.8892	-5.2919	-4.6393	0.6525

Different factors affecting the performance of Li/Na/K incorporated cathode families have been discussed that can be taken into account for the development of future novel cathode materials demonstrating decent performance. The majority of the synthesized Li/Na/K incorporated cathodes demonstrate good electrochemical cyclic stability, capacity retention, rate capability, charge/discharge capacity, etc. Li-incorporated Na-based cathodes show improved performance, which can be attributed to the prevention of phase transformation at high voltages and loss of transition metal from the cathode.

#### 4. Conclusions

Various advancements in the field of Li/Na/K incorporated cathode materials have been observed in the past decades. This research article precisely and briefly reports the various families of Li/Na/K incorporated cathode materials developed for Na/K/Li-ion batteries. Mainly, the effect of Li incorporation in Na/K-based cathode materials and the impact of Na or K addition in Li-based cathode materials have been investigated. In summary, H-grabbing by the nanoclusters of  $\text{Li}_2[\text{SiO-SnO}]$ ,  $\text{Na}_2[\text{SiO-SnO}]$ , or  $\text{K}_2[\text{SiO-SnO}]$  was investigated by first-principles computations of the DFT method. The alterations of charge density illustrated a remarkable charge transfer towards  $\text{Li}_2[\text{SiO-SnO}]$ ,  $\text{Na}_2[\text{SiO-SnO}]$  or  $\text{K}_2[\text{SiO-SnO}]$ . The fluctuation in charge density values demonstrates that the electronic densities were in the boundary of adsorbate/adsorbent atoms during the adsorption status. Besides, thermodynamic parameters describing H-grabbing by alkali metals-based nanoclusters of  $\text{Li}_2[\text{SiO-SnO}]$ ,  $\text{Na}_2[\text{SiO-SnO}]$ , or  $\text{K}_2[\text{SiO-SnO}]$  have been investigated, including the internal process of the adsorbent-adsorbate system.

It is well established that the addition of Li, Na, or K to cell batteries may increase the energy storage in cell batteries. In this work, we explore the effect of Li, Na, or K on SiO-SnO heterocluster. Moreover, hydrogen bond (H-bond) accepting sites by  $\text{Li}_2[\text{SiO-SnO}]$ ,  $\text{Na}_2[\text{SiO-SnO}]$ , or  $\text{K}_2[\text{SiO-SnO}]$  can alleviate parasitic hydrogen evolution in aqueous electrolytes in lithium, sodium, or potassium-ion batteries. Today, it is crucial to distinguish the potential of hydrogen technologies and bring up all perspectives of their performance, from technological progress to economic and social effects. Focused research in this important area, as presented herein, may facilitate understanding the science and governing mechanism of existing Li/Na/K incorporated cathode materials, leading to more innovations and developments to fabricate high-performance future batteries for energy storage applications.

## Institutional Review Board Statement

Not applicable.

## Informed Consent Statement

Not applicable.

## Data Availability Statement

Data supporting the findings of this study are available upon reasonable request from the corresponding author.

## Funding

This research received no external funding.

## Acknowledgments

In successfully completing this paper and its research, the author is grateful to Kastamonu University.

## Conflict of Interest

The author declares no conflict of interest.

## References

1. Antonov, E.N.; Ivanova, A.G.; Krotova, L.I.; Mishakov, G.V.; Popov, V.K. Micronization of Levofloxacin Hemihydrate Using Supercritical Trifluoromethane. *Russ. J. Phys. Chem. B* **2023**, *17*, 1555-1560, <https://doi.org/10.1134/S199079312308002X>.
2. Mollaamin, F. Competitive Intracellular Hydrogen-Nanocarrier Among Aluminum, Carbon, or Silicon Implantation: a Novel Technology of Eco-Friendly Energy Storage using Research Density Functional Theory. *Russ. J. Phys. Chem. B* **2024**, *18*, 805–820, <https://doi.org/10.1134/S1990793124700131>.
3. Mollaamin, F. Features of parametric point nuclear magnetic resonance of metals implantation on boron nitride nanotube by density functional theory/electron paramagnetic resonance. *J. Comput. Theor. Nanosci.* **2014**, *11*, 2393-2398. <https://doi.org/10.1166/jctn.2014.3653>.
4. Mollaamin, F.; Mohammadi, S.; Khalaj, Z.; Monajjemi, M. Computational Modelling of Boron Nitride Nanosheet for Detecting and Trapping of Water Contaminant. *Russ. J. Phys. Chem. B* **2024**, *18*, 67-82, <https://doi.org/10.1134/S1990793124010330>.
5. Agroskin, V.Y.; Bravy, B.G.; Vasiliev, G.K.; Guriev, V.I.; Kashtanov, S.A.; Chernyshev, Y.A. Investigation of the Interaction of Hydrogen Fluoride with Quartz by Measuring Surface Conductivity. *Russ. J. Phys. Chem. B* **2023**, *17*, 1265-1269, <https://doi.org/10.1134/S1990793123060131>.
6. Mollaamin, F.; Monajjemi, M. Corrosion Inhibiting by Some Organic Heterocyclic Inhibitors Through Langmuir Adsorption Mechanism on the Al-X (X = Mg/Ga/Si) Alloy Surface: A Study of Quantum Three-Layer Method of CAM-DFT/ONIOM. *J Bio Tribo Corros.* **2023**, *9*, 33. <https://doi.org/10.1007/s40735-023-00751-y>.
7. Mollaamin, F. Anchoring of 2D layered materials of Ge<sub>5</sub>Si<sub>5</sub>O<sub>20</sub> for (Li/Na/K)-(Rb/Cs) batteries towards Eco-friendly energy storage. *BMC Chemistry.* **2025**, *19*, 233. <https://doi.org/10.1186/s13065-025-01593-0>
8. Tereza, A.M.; Agafonov, G.L.; Anderzhanov, E.K.; Betev, A.S.; Medvedev, S.P.; Mikhalkin, V.N.; Khomik, S.V.; Cherepanova, T.T. Effect of Impurities on Lean Laminar Hydrogen–Air Flames. *Russ. J. Phys. Chem. B* **2023**, *17*, 1294-1299, <https://doi.org/10.1134/S1990793123060246>.
9. Petinov, V.I.; Timin, V.M.; Bozhenko, K.V.; Utenyshev, A.N. The Glow of Mg and Ca Atoms When They Interact with H Atoms. *Russ. J. Phys. Chem. B* **2024**, *18*, 365-368, <https://doi.org/10.1134/S1990793124020301>.

10. Tereza, A.M.; Agafonov, G.L.; Anderzhanov, E.K.; Betev, A.S.; Medvedev, S.P.; Khomik, S.V.; Cherepanova, T.T. Structure of a Lean Laminar Hydrogen–Air Flame. *Russ. J. Phys. Chem. B* **2023**, *17*, 974–978, <https://doi.org/10.1134/S1990793123040309>.
11. Mollaamin, F. Investigating the Treatment of Transition Metals for Ameliorating the Ability of Boron Nitride for Gas Sensing & Removing: A Molecular Characterization by DFT Framework. *Prot Met Phys Chem Surf.* **2024**, *60*, 1050–1063. <https://doi.org/10.1134/S2070205124702502>
12. Rudenko, E.I.; Dohlikova, N.V.; Gatin, A.K.; Sarvadiy, S.Y.; Grishin, M.V. Simulation of Hydrogen and Oxygen Adsorption on Palladium Nanoparticles Located on a Graphite Substrate with Various Defects. *Russ. J. Phys. Chem. B* **2023**, *17*, 845–852, <https://doi.org/10.1134/S1990793123040164>.
13. Mollaamin, F.; Monajjemi, M. Graphene-based resistant sensor decorated with Mn, Co, Cu for nitric oxide detection: Langmuir adsorption & DFT method. *Sens. Rev.* **2023**, *43*, 266–279, <https://doi.org/10.1108/sr-03-2023-0040>.
14. Mollaamin, F.; Monajjemi, M. An Architectural Battery Designed by Substituting Lithium with Second Main Group Metals (Be, Mg, Ca/Cathode) and Hybrid Oxide of Fourth Group Ones (Si, Ge, Sn/Anode) Nanomaterials Towards H<sub>2</sub> Adsorption: A Computational Study. *Nanomaterials* **2025**, *15*, 959. <https://doi.org/10.3390/nano15130959>.
15. Mollaamin, F.; Monajjemi M. Doping of Graphene Nanostructure with Iron, Nickel and Zinc as Selective Detector for the Toxic Gas Removal: A Density Functional Theory Study. *C–Journal of Carbon Research.* **2023**, *9*, 20. <https://doi.org/10.3390/c9010020>.
16. Mollaamin, F. Alkali Metals Doped on Tin-Silicon and Germanium-Silicon Oxides for Energy Storage in Hybrid Biofuel Cells: A First-Principles Study. *Russ. J. Phys. Chem. B.* **2025**, *19*, 722–736. <https://doi.org/10.1134/S1990793125700393>
17. Kayumov, R.R.; Radaeva, A.P.; Krupina, A.A.; Tarusina, K.A.; Lapshin, A.N.; Shmygleva, L.V. Lithium-Conducting Nafion Membrane Plasticized with a DMSO–Sulfolane Mixture. *Russ. J. Phys. Chem. B* **2023**, *17*, 801–809, <https://doi.org/10.1134/S1990793123040097>.
18. Mollaamin, F. Efficiency Enhancement of GaN/InN-Based Solar Cells through Doping with Si, Zn, Ag Elements: A Physico-Chemical Study of Nanosurface by First-Principles Calculation. *Prot Met Phys Chem Surf.* **2025**, *61*, 301–318. <https://doi.org/10.1134/S2070205125700212>
19. Troshin, K.Y.; Rubtsov, N.M.; Tsvetkov, G.I.; Chernysh, V.I.; Shamshin, I.O. Features of Ignition of Mixtures of Hydrogen With Hydrocarbons (C<sub>2</sub>, C<sub>3</sub>, C<sub>5</sub>) Over Rhodium and Palladium at Pressures of 1–2 atm. *Russ. J. Phys. Chem. B* **2023**, *17*, 979–985, <https://doi.org/10.1134/S1990793123040310>.
20. Troshin, K.Y.; Rubtsov, N.M.; Tsvetkov, G.I.; Chernysh, V.I.; Shamshin, I.O. Ignition Limits of Hydrogen–Methane–Air Mixtures Over Metallic Rhodium at a Pressure of up to 2 atm. *Russian Russ. J. Phys. Chem. B* **2023**, *17*, 433–438, <https://doi.org/10.1134/S1990793123020185>.
21. Xiong, Q.Q. First-Principles Prediction on Structural, Elastic, Mechanical, and Electronic Properties of Chalcogenide Perovskite CaZrS<sub>3</sub> under Pressure. *Russ. J. Phys. Chem. B* **2024**, *18*, 638–644, <https://doi.org/10.1134/S1990793124700155>.
22. Mollaamin, F.; Monajjemi, M. Harmonic Linear Combination and Normal Mode Analysis of Semiconductor Nanotubes Vibrations. *J. Comput. Theor. Nanosci.* **2015**, *12*, 1030–1039, <https://doi.org/10.1166/jctn.2015.3846>.
23. Yuan, X.; Tan, X.; Liu, B. Structural, Mechanical, Electronic and Optical Properties of Spinel ZnAl<sub>2</sub>O<sub>4</sub> Underpressure from First-Principles Calculations. *Russ. J. Phys. Chem. B* **2023**, *17*, 886–895, <https://doi.org/10.1134/S1990793123040322>.
24. Trakhtenberg, L.I. Sensor Layers Based on Semiconductor Nanoparticles and Their Electronic Structure. *Russ. J. Phys. Chem. B* **2023**, *17*, 600–607, <https://doi.org/10.1134/S1990793123030144>.
25. Mollaamin, F.; Monajjemi, M. Graphene Embedded with Transition Metals for Capturing Carbon Dioxide: Gas Detection Study Using QM Methods. *Clean Technol.* **2023**, *5*, 403–417. <https://doi.org/10.3390/cleantechnol5010020>.
26. Mollaamin, F.; Monajjemi, M.; Salemi, S.; Baei, M.T. A Dielectric Effect on Normal Mode Analysis and Symmetry of BNNT Nanotube. *Fuller. Nanotub. Carbon Nanostructures* **2011**, *19*, 182–196, <https://doi.org/10.1080/15363831003782932>.
27. Mollaamin, F.; Monajjemi, M. Determination of GaN nanosensor for scavenging of toxic heavy metal ions (Mn<sup>2+</sup>, Zn<sup>2+</sup>, Ag<sup>+</sup>, Au<sup>3+</sup>, Al<sup>3+</sup>, Sn<sup>2+</sup>) from water: Application of green sustainable materials by molecular modeling approach. *Comput. Theor. Chem.* **2024**, 1237, 114646, <https://doi.org/10.1016/j.comptc.2024.114646>.

28. Mollaamin, F.; Monajjemi, M. In Silico-DFT Investigation of Nanocluster Alloys of Al-(Mg, Ge, Sn) Coated by Nitrogen Heterocyclic Carbenes as Corrosion Inhibitors. *J. Clust. Sci.* **2010**, *34*, 2901–2918, <https://doi.org/10.1007/s10876-023-02436-5>.
29. Yodsins, N.; Sakagami, H.; Udagawa, T.; Ishimoto, T.; Jungsuttiwong, S.; Tachikawa, M. Metal-doped carbon nanocones as highly efficient catalysts for hydrogen storage: Nuclear quantum effect on hydrogen spillover mechanism. *Mol. Catal.* **2021**, *504*, 111486, <https://doi.org/10.1016/j.mcat.2021.111486>.
30. Galashev, A.E. Computer Simulation of a Silicene Anode on a Silicene Carbide Substrate. *Russ. J. Phys. Chem. B* **2023**, *17*, 113–121, <https://doi.org/10.1134/S1990793123010190>.
31. Wei, T.; Zhou, Y.; Sun, C.; Guo, X.; Xu, S.; Chen, D.; Tang, Y. An intermittent lithium deposition model based on CuMn-bimetallic MOF derivatives for composite lithium anode with ultrahigh areal capacity and current densities. *Nano Res.* **2024**, *17*, 2763–2769, <https://doi.org/10.1007/s12274-023-6187-8>.
32. Yao, K.; Ling, M.; Liu, G.; Tong, W. Chemical Reduction Synthesis and Electrochemistry of Si–Sn Nanocomposites as High-Capacity Anodes for Li-Ion Batteries. *J. Phys. Chem. Lett.* **2018**, *9*, 5130–5134, <https://doi.org/10.1021/acs.jpcclett.8b02066>.
33. Cardella, U.; Decker, L.; Sundberg, J.; Klein, H. Process optimization for large-scale hydrogen liquefaction. *Int. J. Hydrogen Energy* **2017**, *42*, 12339–12354, <https://doi.org/10.1016/j.ijhydene.2017.03.167>.
34. Hammad, A.; Dincer, I. Analysis and assessment of an advanced hydrogen liquefaction system. *Int. J. Hydrogen Energy* **2018**, *43*, 1139–1151, <https://doi.org/10.1016/j.ijhydene.2017.10.158>.
35. Kim, O.A.; Bogdan, T.V.; Koklin, A.E.; Bogdan, V.I. Interaction of Carbon Dioxide with Hydrogen on Supported Fe,Cr-Containing Catalysts. *Russ. J. Phys. Chem. B* **2022**, *16*, 1218–1220, <https://doi.org/10.1134/S1990793122070107>.
36. Qyyum, M.A.; Chaniago, Y.D.; Ali, W.; Saulat, H.; Lee, M. Membrane-Assisted Removal of Hydrogen and Nitrogen from Synthetic Natural Gas for Energy-Efficient Liquefaction. *Energies* **2020**, *13*, 5023, <https://doi.org/10.3390/en13195023>.
37. Davtyan, A.H.; Manukyan, Z.H.; Arsentev, S.D.; Tavadyan, L.A.; Arutyunov, V.S. Study of the Potential Energy Surface of Reactions in a System Containing I-Propyl and N-Propyl Radicals. *Russ. J. Phys. Chem. B* **2024**, *18*, 461–467, <https://doi.org/10.1134/S1990793124020209>.
38. Yu, X.; Zhang, X.; Wang, H.; Wang, Z.; Feng, G. High-Coverage H<sub>2</sub> Adsorption on the Reconstructed Cu<sub>2</sub>O(111) Surface. *J. Phys. Chem. C* **2017**, *121*, 22081–22091, <https://doi.org/10.1021/acs.jpcc.7b06361>.
39. Mollaamin, F.; Monajjemi, M. Transition metal (X = Mn, Fe, Co, Ni, Cu, Zn)-doped graphene as gas sensor for CO<sub>2</sub> and NO<sub>2</sub> detection: a molecular modeling framework by DFT perspective. *J. Mol. Model.* **2023**, *29*, 119, <https://doi.org/10.1007/s00894-023-05526-3>.
40. Rivard, E.; Trudeau, M.; Zaghbi, K. Hydrogen Storage for Mobility: A Review. *Materials* **2019**, *12*, 1973, <https://doi.org/10.3390/ma12121973>.
41. Mollaamin, F.; Monajjemi, M. Electric and Magnetic Evaluation of Aluminum–Magnesium Nanoalloy Decorated with Germanium Through Heterocyclic Carbenes Adsorption: A Density Functional Theory Study. *Russ. J. Phys. Chem. B* **2023**, *17*, 658–672, <https://doi.org/10.1134/S1990793123030223>.
42. Mollaamin, F.; Monajjemi, M. Nanomaterials for Sustainable Energy in Hydrogen-Fuel Cell: Functionalization and Characterization of Carbon Nano-Semiconductors with Silicon, Germanium, Tin or Lead through Density Functional Theory Study. *Russ. J. Phys. Chem. B* **2024**, *18*, 607–623, <https://doi.org/10.1134/S1990793124020271>.
43. Mollaamin, F.; Shahriari, S.; Monajjemi, M. Influence of Transition Metals for Emergence of Energy Storage in Fuel Cells through Hydrogen Adsorption on the MgAl Surface. *Russ. J. Phys. Chem. B* **2024**, *18*, 398–418, <https://doi.org/10.1134/S199079312402026X>.
44. Agroskin, V.Y.; Bravy, B.G.; Vasiliev, G.K.; Guriev, V.I.; Kashtanov, S.A.; Makarov, E.F.; Sotnichenko, S.A.; Chernyshev, Y.A. Influence of Quartz on The Storage of Hydrogen Fluorine Mixtures. *Russ. J. Phys. Chem. B* **2022**, *16*, 596–601, <https://doi.org/10.1134/S1990793122040029>.
45. Yanai, T.; Tew, D.P.; Handy, N.C. A new hybrid exchange–correlation functional using the Coulomb-attenuating method (CAM-B3LYP). *Chem. Phys. Lett.* **2004**, *393*, 51–57, <https://doi.org/10.1016/j.cplett.2004.06.011>.
46. Henkelman, G.; Arnaldsson, A.; Jónsson, H. A fast and robust algorithm for Bader decomposition of charge density. *Comput. Mater. Sci.* **2006**, *36*, 354–360, <https://doi.org/10.1016/j.commatsci.2005.04.010>.
47. Bader, R.F.W.; Bader, R.F. *Atoms in Molecules: A Quantum Theory*. Clarendon Press: Oxford, United Kingdom, **1990**.

48. Mollaamin, F.; Monajjemi, M. Structural, Electromagnetic and Thermodynamic Analysis of Ion Pollutants Adsorption in Water by Gallium Nitride Nanomaterial: a Green Chemistry Application. *Russ. J. Phys. Chem. B* **2024**, *18*, 533-548, <https://doi.org/10.1134/S199079312402012X>.
49. Mollaamin, F. Computational Methods in the Drug Delivery of Carbon Nanocarriers onto Several Compounds in Sarraceniaceae Medicinal Plant as Monkeypox Therapy. *Computation* **2023**, *11*, 84. <https://doi.org/10.3390/computation11040084>
50. Mollaamin, F.; Monajjemi, M. Selectivity and Sensitivity Evaluation of Embedded BN-Nanostructure as a Gas Detector for Air Pollution Scavenging: a Theoretical Study. *Russ. J. Phys. Chem. B.* **2024**, *18*, 1177–1198. <https://doi.org/10.1134/S1990793124700507>.
51. Monajjemi, M.; Noei, M.; Mollaamin, F. Design of fMet-tRNA and Calculation of its Bonding Properties by Quantum Mechanics. *Nucleos. Nucleot. Nucleic Acids* **2010**, *29*, 676–683, <https://doi.org/10.1080/15257771003781642>.
52. Mollaamin, F.; Monajjemi, M. The influence of Sc, V, Cr, Co, Cu, Zn as ferromagnetic semiconductors implanted on B5N10-nanocarrier for enhancing of NO sensing: An environmental eco-friendly investigation. *Comput. Theor. Chem.* **2024**, *1237*, 114666, <https://doi.org/10.1016/j.comptc.2024.114666>.
53. Shahriari, S.; Mollaamin, F.; Monajjemi, M. Increasing the Performance of  $\{(1-x-y) \text{LiCo}_{0.3}\text{Cu}_{0.7}\} (\text{Al and Mg doped}) \text{O}_2\}$ ,  $x\text{Li}_2\text{MnO}_3$ ,  $y\text{LiCoO}_2$  Composites as Cathode Material in Lithium-Ion Battery: Synthesis and Characterization. *Micromachines* **2023**, *14*, 241, <https://doi.org/10.3390/mi14020241>.
54. Mollaamin, F.; Monajjemi, M. Trapping of toxic heavy metals from water by GN–nanocage: Application of nanomaterials for contaminant removal technique. *J. Mol. Struct.* **2024**, *1300*, 137214, <https://doi.org/10.1016/j.molstruc.2023.137214>.
55. Mollaamin, F.; Ilkhani, A.; Sakhaei, N.; Bonsakhteh, B.; Faridchehr, A.; Tohidi, S.; Monajjemi, M. Thermodynamic and solvent effect on dynamic structures of nano bilayer-cell membrane: Hydrogen bonding study. *J. Comput. Theor. Nanosci.* **2015**, *12*, 3148-3154, <https://doi.org/10.1166/jctn.2015.4092>.
56. Mollaamin, F.; Monajjemi, M. Boron nitride doped with transition metals for carbon monoxide detection: a promising nanosensor for air cleaning. *Sens. Rev.* **2024**, *44*, 179-193, <https://doi.org/10.1108/SR-01-2024-0066>.
57. Mollaamin, F.; Monajjemi, M. Perspective of Clean Energy-saving by Semiconducting Quantum Dot Nanomaterials through Photoelectric and Density of States Analysis. *J. Fluoresc.* **2025**. <https://doi.org/10.1007/s10895-025-04207-z>.
58. Mollaamin, F.; Monajjemi, M. In Situ Ti-Embedded SiC as Chemiresistive Nanosensor for Safety Monitoring of CO, CO<sub>2</sub>, NO, NO<sub>2</sub>: Molecular Modelling by Conceptual Density Functional Theory. *Russ. J. Phys. Chem. B* **2024**, *18*, 49–66, <https://doi.org/10.1134/S1990793124010159>.
59. Mollaamin, F.; Monajjemi, M. Adsorption ability of Ga<sub>5</sub>N<sub>10</sub> nanomaterial for removing metal ions contamination from drinking water by DFT. *Int. J. Quantum Chem.* **2024**, *124*, e27348, <https://doi.org/10.1002/qua.27348>.
60. Mollaamin, F.; Monajjemi, M. Molecular modelling framework of metal-organic clusters for conserving surfaces: Langmuir sorption through the TD-DFT/ONIOM approach. *Mol. Simul.* **2023**, *49*, 365–376, <https://doi.org/10.1080/08927022.2022.2159996>.
61. Feskov, S.V. Method of Splitting Polarization Coordinates for the Description of Ultrafast Multistage Electron Transfer in a Non-Debye Medium. *Russ. J. Phys. Chem. B* **2024**, *18*, 1–8, <https://doi.org/10.1134/S1990793124010081>.
62. Frisch, M.J.; Trucks, G.W.; Schlegel, H.B.; Scuseria, G.E.; Robb, M.A.; Cheeseman, J.R.; Scalmani, G.; Barone, V.; Petersson, G.A.; Nakatsuji, H.; Li, X.; Caricato, M.; Marenich, A.V.; Bloino, J.; Janesko, B.G.; Gomperts, R.; Mennucci, B.; Hratchian, H.P.; Ortiz, J. V.; Izmaylov, A. F.; Sonnenberg, J.L.; Williams-Young, D.; Ding, F.; Lipparini, F.; Egidi, F.; Goings, J.; Peng, B.; Petrone, A.; Henderson, T.; Ranasinghe, D.; Zakrzewski, V.G.; Gao, J.; Rega, N.; Zheng, G.; Liang, W.; Hada, M.; Ehara, M.; Toyota, K.; Fukuda, R.; Hasegawa, J.; Ishida, M.; Nakajima, T.; Honda, Y.; Kitao, O.; Nakai, H.; Vreven, T.; Throssell, K.; Montgomery, J.A., Jr.; Peralta, J.E.; Ogliaro, F.; Bearpark, M.J.; Heyd, J.J.; Brothers, E.N.; Kudin, K.N.; Staroverov, V.N.; Keith, T.A.; Kobayashi, R.; Normand, J.; Raghavachari, K.; Rendell, A.P.; Burant, J.C.; Iyengar, S.S.; Tomasi, J.; Cossi, M.; Millam, J.M.; Klene, M.; Adamo, C.; Cammi, R.; Ochterski, J.W.; Martin, R.L.; Morokuma, K.; Farkas, O.; Foresman, J.B.; Fox, D.J. Gaussian 16, Revision C.01, Gaussian, Inc., Wallingford CT, **2016**.
63. Dennington, R.; Keith, T.A.; Millam, J.M. GaussView 6.0. 16. SemicheM Inc., Shawnee Mission, **2016**.

64. Xu, Z.; Qin, C.; Yu, Y.; Jiang, G.; Zhao, L. First-principles study of adsorption, dissociation, and diffusion of hydrogen on  $\alpha$ -U (110) surface. *AIP Adv.* **2024**, *14*, 055114, <https://doi.org/10.1063/5.0208082>.
65. O'Boyle, N.M.; Tenderholt, A.L.; Langner, K.M. cclib: A library for package-independent computational chemistry algorithms. *J. Comput. Chem.* **2008**, *29*, 839-845, <https://doi.org/10.1002/jcc.20823>.
66. Matta, C.F.; Ayers, P.W.; Cook, R. The Physics of Electron Localization and Delocalization. In *Electron Localization-Delocalization Matrices*, Matta, C.F., Ayers, P.W., Cook, R., Eds.; Springer International Publishing: Cham, **2024**; pp. 7-20, [https://doi.org/10.1007/978-3-031-51434-0\\_2](https://doi.org/10.1007/978-3-031-51434-0_2).
67. Bader, R.F.W. The zero-flux surface and the topological and quantum definitions of an atom in a molecule. *Theor. Chem. Acc.* **2001**, *105*, 276-283, <https://doi.org/10.1007/s002140000233>.
68. Lu, T.; Chen, F. Multiwfn: A multifunctional wavefunction analyzer. *J. Comput. Chem.* **2012**, *33*, 580-592, <https://doi.org/10.1002/jcc.22885>.
69. Lu, T. A comprehensive electron wavefunction analysis toolbox for chemists, Multiwfn. *J. Chem. Phys.* **2024**, *161*, 082503, <https://doi.org/10.1063/5.0216272>.
70. Becke, A.D.; Edgecombe, K.E. A simple measure of electron localization in atomic and molecular systems. *J. Chem. Phys.* **1990**, *92*, 5397-5403, <https://doi.org/10.1063/1.458517>.
71. Savin, A.; Jepsen, O.; Flad, J.; Andersen, O.K.; Preuss, H.; von Schnering, H.G. Electron Localization in Solid-State Structures of the Elements: the Diamond Structure. *Angew. Chem. Int. Ed. Engl.* **1992**, *31*, 187-188, <https://doi.org/10.1002/anie.199201871>.

### **Publisher's Note & Disclaimer**

The statements, opinions, and data presented in this publication are solely those of the individual author(s) and contributor(s) and do not necessarily reflect the views of the publisher and/or the editor(s). The publisher and/or the editor(s) disclaim any responsibility for the accuracy, completeness, or reliability of the content. Neither the publisher nor the editor(s) assume any legal liability for any errors, omissions, or consequences arising from the use of the information presented in this publication. Furthermore, the publisher and/or the editor(s) disclaim any liability for any injury, damage, or loss to persons or property that may result from the use of any ideas, methods, instructions, or products mentioned in the content. Readers are encouraged to independently verify any information before relying on it, and the publisher assumes no responsibility for any consequences arising from the use of materials contained in this publication.